Volume 16 | Number 1 | 7 January 2014 | Pages 1–124

CrystEngComm

www.rsc.org/crystengcomm

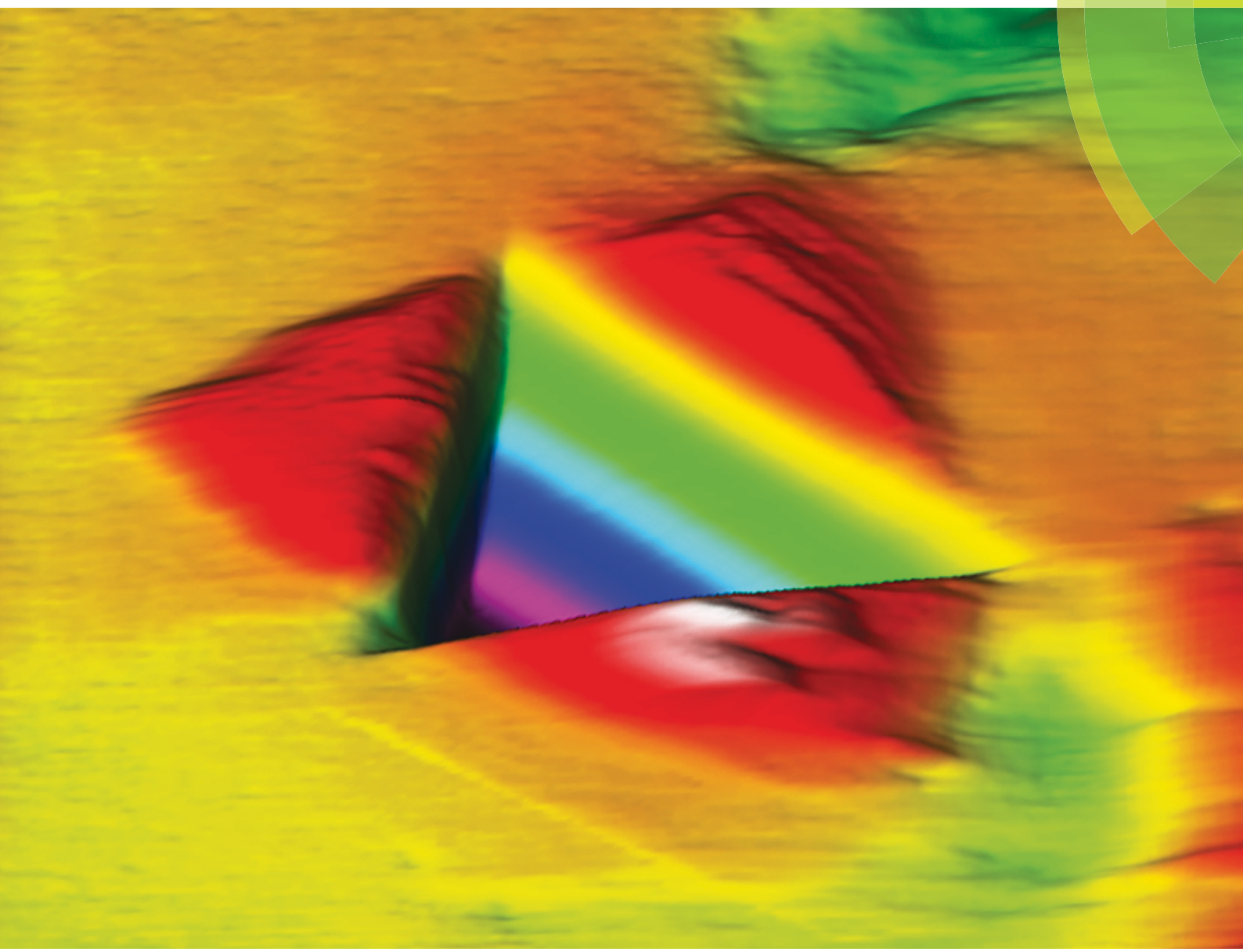

ROYAL SOCIETY OF CHEMISTRY

COVER ARTICLE
Ramamurty and Jang
Nanoindentation for probing the mechanical behavior of molecular crystals–a review of the technique and how to use it

CrystEngComm

HIGHLIGHT

View Article Online
View Journal | View Issue

Nanoindentation for probing the mechanical behavior of molecular crystals–a review of the technique and how to use it

Cite this: *CrystEngComm*, 2014, **16**, 12

Upadrasta Ramamurty*[ab] and Jae-il Jang*[c]

Received 28th June 2013,
Accepted 11th September 2013

DOI: 10.1039/c3ce41266k

www.rsc.org/crystengcomm

Nanoindentation is a technique which can be used to measure the mechanical properties of materials with high precision, even when they are only available in small quantities. As a result of this, nanoindentation has gained the attention of the crystal engineering community, who are not only interested in measuring the properties of single crystals of organic, inorganic and hybrid structures, but also wish to correlate the measured responses with the underlying structural features and intermolecular interactions. Keeping this emerging interest in view, a brief overview of the technique, with particular emphasis on the procedures for conducting experiments and analyzing the resulting data, is presented in this *Tutorial style Highlight*. The precautions that need to be taken and the properties that one can measure using nanoindentation are highlighted. This paper ends with a brief summary of the recent additional features that have been added to this technique and an outlook for nanoindentation within the context of crystal engineering.

1. Introduction

The indentation test for measuring the hardness of solids is one of the oldest among all the mechanical testing techniques and is routinely used as a quality control tool in metallurgical industries. The scientific concepts associated with this test are typically referred to as 'contact mechanics.' The fundamentals of elastic contact were first examined in the late nineteenth century by Boussinesq[1] and Hertz.[2] The first widely accepted and standardized indentation test was proposed in 1900 by Brinell[3] who used a hardened steel ball for indentation, and defined the Brinell hardness as the applied load, P, divided by the surface area of the impression created, A. In 1908, Meyer[4] suggested a more technically correct definition of hardness; P divided by the 'projected area' of the impression, this has now become the standard method for estimating hardness, H. Later, other alternatives including the Vickers, Knoop and Rockwell hardness tests, which employ indenters of different geometries, were developed and standardized.[5]

Instrumented indentation tests, wherein P and the corresponding depth of penetration, h, are continuously measured and subsequently analyzed, were first developed in Russia in the 1970s.[6] These tests are also referred to as either load- or depth-sensing indentations. With these, it is possible to estimate the elastic properties – in addition to H – of the material being indented. The advent of instruments in the early 1980s which could produce submicron-sized indentations, with the capability for high precision measurement of P and h, led to development of the 'nanoindentation' technique, which has proven to be a powerful tool for measuring the mechanical properties of materials that are available in only small volumes.[7,8] Examples of such materials are thin films deposited on a substrate, coatings and small crystals. Unlike conventional hardness tests, nanoindentation measures mechanical properties by analyzing the P–h responses that are recorded during entire loading and unloading sequences. This alleviates the necessity to image the indentations, which would be a difficult task since the indents are very small in size (typically sub-micron in length, or width, or both) and hence are not easy to locate for *post facto* imaging. The International Standards Organization (ISO, standard no. 14577 Part 1–4)[9] as well as the American Society for Testing of Materials (ASTM Standard no. E2540)[10] prescribe the standard methods for conducting nanoindentation tests.

In the recent past, nanoindentation has been employed by chemists for evaluating the mechanical properties of crystals of organic, inorganic and metal–organic framework (MOF) materials.[11–15] It has been shown that factors like anisotropy in the molecular interactions of saccharin, the shear stability of aspirin and caffeine polymorphs, molecular layer sliding and migration in layered organic donor–

[a] *Department of Materials Engineering, Indian Institute of Science, Bangalore 560012, India. E-mail: ramu@materials.iisc.ernet.in*
[b] *Center of Excellence for Advanced Materials Research, King Abdulaziz University, Jeddah 21589, Saudi Arabia*
[c] *Division of Materials Science and Engineering, Hanyang University, Seoul 133-791, Korea. E-mail: jijang@hanyang.ac.kr*

acceptor complexes, the stiffness of different types of bonds in MOFs and elastic modulus alternation in alkanedicarboxylic acids, can be explored with the aid of this technique (summarized in a recent review).[14] An additional advantage of nanoindentation is the ability to position the indenter at specified locations on the materials being tested, which facilitates probing of the properties of microstructural constituents, and in turn, assessment of structural inhomogeneities such as intergrowth of secondary phases or polymorphs, for example in aspirin.[16] This makes nanoindentation a technique which can complement others, like X-ray diffraction, for development of new insights into phenomena like polymorphism, which are of immense interest to crystal engineers. In keeping with the growing interest in nanoindentation, we provide here an overview of the technique with particular emphasis on how it can be utilized by a researcher who is interested in using it in his/her research for the first time.

This paper is organized as follows: in the next section (section 2) we give details on how to select an instrument and then conduct nanoindentation experiments, this is followed by procedures for analyzing the results so as to obtain different mechanical properties (section 3), recent advances in instrumentation for additional testing options are briefly discussed in section 4 before the summary.

2. Nanoindentation experiments

2.1. Instrument choices and selection

The nanoindentation apparatus is a fairly sophisticated instrument and several commercial instrument makers, who employ differing design principles, manufacture it. When making a choice between these, basic features like the maximum load and displacement ratings, the resolution and precision of the measurements, machine stiffness, stability (in terms of thermal drift), noise floor, and most importantly user friendliness and cost, need to ascertained. Significant progress has been made by manufacturers of nanoindenters in the last two decades, which means most of the aforementioned features are broadly similar across different instruments, but subtle differences do exist. There are many additional capabilities – such as high temperature nanoindentation – being developed and offered, which vary from instrument to instrument.

An important consideration during the selection of an instrument is its capability for imaging the indents, which often becomes essential, either to judge the validity of an experiment or to examine whether there is any pile-up or cracking of the material around the indents. In some instruments, the same indenter tip can be employed to scan the indent with a reasonable degree of resolution, whereas in others an atomic force microscope (AFM) can be attached which works in tandem with the instrument for imaging purposes. Once a suitable instrument has been procured, it is important to locate it in a vibration, dust and thermal-fluctuation free environment.

The standard tip used for nanoindentation is a Berkovich tip, but tips with different geometries can be mounted relatively easily. Generally the tips are made of diamond, but for specific purposes tips made of Zircon, boron-doped diamond, hardened steel and tungsten can be utilized. The tips – especially sharp ones – tend to wear with usage and become blunt in the process, hence they are the only 'consumables' associated with this technique.

2.2. Sample sizes and surface preparation

A common assumption – stemming from the fact that 'nano' is in the technique's name – is that nano-dimensional specimens in particulate, film, tube or rod form can be tested. This is not correct, and in reality a stand-alone specimen should at least be 0.1×0.1 mm^2 in cross-section and a few hundred nm thick. The latter, as a general rule, should be at least ten times (in the case of hard and stiff materials) or twenty times (for compliant and soft materials) the maximum depth of penetration, h_{max}. Satisfying this condition means that the substrate does not influence the stress and strain fields of indentation, and the measured response is exclusively that of the material being probed. Since sub-micron thick specimens are difficult to handle, they can only be tested in a thin film form (deposited on a rigid substrate). If free-standing specimens are to be tested, they need to be at least sub-mm in size and should have flat surfaces. Sometimes, it may be possible to disperse micron-sized specimens in a matrix. In such a scenario, one has to ensure that the matrix's mechanical properties are far superior, *i.e.*, stiffer and harder, to those of the material being tested.

Preparation of the test surface which is to be probed with the nanoindenter is an extremely important first step, as the final surface finish can exert significant influence on the results obtained. There are two important points to keep in mind here. Firstly, the surface should be as smooth as possible, because (a) loading should be normal to the surface and (2) the effective contact area is estimated assuming that the surface is flat. Thus, if the amplitude of the surface roughness is comparable to the contact diameter, indentations at 'valleys' or 'peaks' will result in underestimation or overestimation, respectively, of the true contact area. Secondly, surface preparation should be performed in such a way that possible alteration of the surface in terms of its mechanical properties (due to heat or work hardening generated upon polishing) or chemistry (due to absorption of chemicals in the polishing media, evaporation of elements in the sample, and/or hydration/dehydration) are minimized. While electrolytic polishing is preferred to mechanical polishing for obtaining a good surface finish in metals and alloys, such a method may not be suitable for organic/inorganic crystals. In these cases, even gentle polishing may induce surface defects. The best way, perhaps, would be to find flat regions on the surface of the crystals and indent there. Usually, the major faces of crystals tend to be smooth, so obtaining a flat surface may not be a problem. In cases

where the natural facets are not smooth enough for indentation, careful polishing after cold mounting, as described by Tan *et al.*,[12e] may be performed. In some instances, cleaving the crystal with a sharp blade may create a sufficiently smooth surface. Some small crystals tend to attach to the surface of large crystals during solution synthesis; these need to be removed using an appropriate method (such as ultrasonic cleaning of the crystal in paraffin oil).

Another important aspect with respect to specimen preparation is that the sample must be held rigidly for indentation, ensuring that the displacement that is measured is the true depth of penetration. (If the crystals are not held rigidly or if a compliant substrate is utilized, the measured h may include other displacements, such as that associated with the substrate deformation.) For crystals, this means using an appropriate, strong adhesive for mounting. In such cases, only a thin layer of adhesive should be applied and care should be taken to cure it sufficiently, ensuring that it is as hard as possible.

2.3. Thermal drift and other effects

Since the depth sensor of a nanoindenter is highly sensitive – a necessity given that it has to measure with sub-nm resolution – thermally-induced displacement drift due to ambient temperature fluctuations is a major factor which could influence the results in a substantial manner. Two types of drift due to thermal expansion or contraction can occur; the first is displacement within the test sample, and the second is a change in the dimensions of the instrument. To minimize thermal drift, the instrument should be held at a constant temperature during the course of the test, or the displacement drift should be accounted for. Typically, one should not start a nanoindentation test until the thermal drift is lower than 0.05 nm s^{-1}, and care should be taken to maintain this status during the test. A hold period at the maximum load or at near-completion of unloading may also be used to estimate drift in any given experiment, allowing the measured P–h data to be corrected accordingly.

Another factor to keep in mind, particularly in the context of testing organics, is the hydration level of the sample as well as the ambient humidity. Many organic materials tend to dehydrate in dry environments, whereas some organics may absorb moisture in a very humid environment. Such changes in the water content of the sample can exert a significant influence on its measured mechanical properties.[17–19] Hence, it is important to keep track of the relative hydration levels in the specimen as well as the humidity in the nanoindenter chamber, and make sure that the tests are performed without an inordinate delay between synthesis of the crystals and their testing.

2.4. Controllable testing parameters

One may need to carefully choose the testing parameters, such as the maximum load (P_{max}) or the maximum displacement (h_{max}), and the rate at which the indentations are performed. Just as in uniaxial tensile tests, nanoindentation experiments can be performed either in load- or displacement-control. In the former, the loading and unloading rates (dP/dt) and P_{max} are prescribed. In displacement control mode, which has been developed somewhat recently, dh/dt and h_{max} are fixed, and the indentation rate is set as the displacement rate; *i.e.*, the depth variation is kept as constant as possible by the feedback indenter position controller for every indentation segment. If the deformation behavior of the material is homogeneous, the P–h curves obtained under both the modes will be identical. However, in the case where deformation is either inhomogeneous or intermittent, the measured P–h responses will depend on the mode of control. For example, while one may note discrete displacement bursts (so-called 'pop-ins', which will be discussed in the next section) in the P–h curves obtained in load control, the same bursts will be reflected as load-drops in tests performed under displacement control.

In either mode, one has to ensure that h_{max} is less than 10% of the test piece thickness, while ensuring that it allows for collecting sufficient amounts of data for a meaningful curve. In addition, at very shallow depths, and for nanoindentation with a sharp indenter, the hardness H increases significantly as h (or P) decreases, which is referred to as the indentation size effect.[20–22] Thus, the nanoindentation hardness may not be comparable in a one-to-one fashion to the macro-scale hardness measured from conventional hardness tests. The rates of loading, dP/dt or dh/dt, and the indentation strain rate given by $h^{-1}(dh/dt)$ are another set of important experimental variables, and one should consider the rate effects carefully as they affect the test results markedly. If the rates are very high, the h_{max} at P_{max} decreases (and thus H increases) due to material inertial effects and the possibility that some portion of plastic flow could be delayed into the subsequent load-hold at P_{max}. On the other hand, very low rates are not desirable either, due to (1) thermal drift effects and (2) the occurrence of dynamic creep (*i.e.*, time-dependent deformation in the specimen during the loading sequence). The mechanical behavior of many materials is rate sensitive, so one can investigate such a behavior by conducting a systematic study with the loading rate as an experimental variable. In fact, it may be possible to extract fundamental information like the activation energy and volume of deformation from such studies.

3. Extraction of properties

The three basic attributes of a material – in terms of its mechanical behavior – are its stiffness, strength and toughness. These properties reflect, broadly, the resistance offered by the solid to elastic and plastic deformations, and cracking, respectively. The elastic modulus, E, hardness, H, and indentation fracture toughness, K_i, are the respective properties, indicative of these resistance behaviors, which can be

measured using the nanoindentation technique as detailed below.

3.1. Hardness and Young's modulus

The typical goal of a nanoindentation experiment is to estimate the H and E of a material from its P–h curve (a typical example is shown in Fig. 1), recorded during testing. The most popular method for doing this is proposed by Oliver and Pharr[23] according to which, H (which is equal to the mean contact pressure, p_m) is defined as:

$$H = \frac{P_{max}}{A_C} \quad (1)$$

where A_C is the projected contact area. A_C is a geometrical function of the contact depth, h_C. For an ideal Berkovich tip, $A_C = 24.5h_C^2$. However, even fresh tips tend to have a finite radius (typically around 50 nm) and get more and more blunt as a function of usage. Hence, the tips need to be calibrated from time to time to evaluate the functional relationship between A_C and h_C. Oliver and Pharr[23] proposed that the contact depth can be given by:

$$h_C = h_{max} - \omega\frac{P_{max}}{S} \quad (2)$$

where ω is a geometric parameter; ω = 0.72 for a cone, 0.75 for a rounded tip, and 1 for a flat punch. Note that ω = 0.75 for the Berkovich tip, which is a three-sided pyramid (somewhat analogous to a cone) and is the tip most widely used in nanoindentation experiments. The unloading stiffness, S, is the initial slope of the unloading curve (see Fig. 1) and is estimated as follows. First, the unloading curve is fitted to the power-law relation, $P = B(h - h_f)^m$ where B and m are fitting parameters, and h_f is the final displacement after complete unloading (also determined by curve fitting). Then, S is determined by differentiating this relation and setting $h = h_{max}$ such that $S = dP/dh|_{h=h_{max}}$.

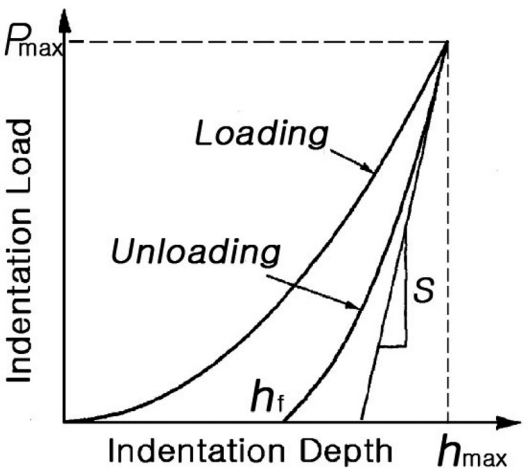

Fig. 1 Typical example of a load–displacement curve recorded during instrumented indentation.

From S and A_C, it is also possible to determine the reduced modulus, E_r, (which is also referred to as the effective modulus) of the indented material, through the elastic contact theory: [23,24]

$$E_r = \frac{1}{\beta}\frac{\sqrt{\pi}}{2}\frac{S}{\sqrt{A_C}} \quad (3)$$

where β is a constant that depends on the indenter geometry. Note that the proper value of β is known only for the commonly used Berkovich indenter (1.034), and the dependency of β on the indenter angle is still unclear, which may lead miscalculation of H for other pyramidal indenters with different included angles (*e.g.* a cube-corner indenter). E_r accounts for the fact that elastic deformation during indentation occurs in both the specimen and the indenter, given by

$$\frac{1}{E_r} = \frac{1-\nu_s^2}{E_s} + \frac{1-\nu_i^2}{E_i} \quad (4)$$

where ν is Poisson's ratio, with the subscripts, s and I, indicating the sample and the indenter. For a diamond indenter, E_i = 1141 GPa and ν_i = 0.07 (ref. 23 and 25) and hence $E_s \approx E_r$ for relatively complaint organic crystals. Although eqn (3) was originally derived for a conical indenter, Pharr *et al.*[26] verified that it can be applied to any indenter which can be described as a body of revolution of a smooth function. It is important to highlight here that E_s is estimated from the unloading segment of the P–h curve as it reflects the elastic unloading of the material underneath the indenter. Thus, if phase transformation or cracking occur during the loading segment, the estimated modulus may reflect that of the transformed or cracked solid. In the latter case, since cracking induces considerable compliance in the specimen, the estimated E_s is likely to be substantially lower than the actual value, and hence is not valid. Another factor to consider is that the analysis presented above is for isotropic materials and single crystals naturally tend to be anisotropic. Thus, the value of ν, which is typically assumed to be in the range of 0.3 to 0.4, may also be directionally-dependent.

There are many issues to be considered in the estimation of the hardness H. Among them, the effect of 'pile-up' is the most relevant in the current context.† When the material underneath the indenter deforms extensively, plastic flow occurs against the indenter faces and piles-up around indentation impression (see Fig. 2 for images of pile-up around the indenter and images without any pile-up). Such pile-up is not taken into consideration in the Oliver–Pharr method, which can induce an overestimation of the calculated H. In such

† In certain materials, which have high modulus and strength, another phenomenon known as sink-in could occur. In such cases, the indentation impressions will appear similar to those of pinned cushions, with the edges concaving inwards.

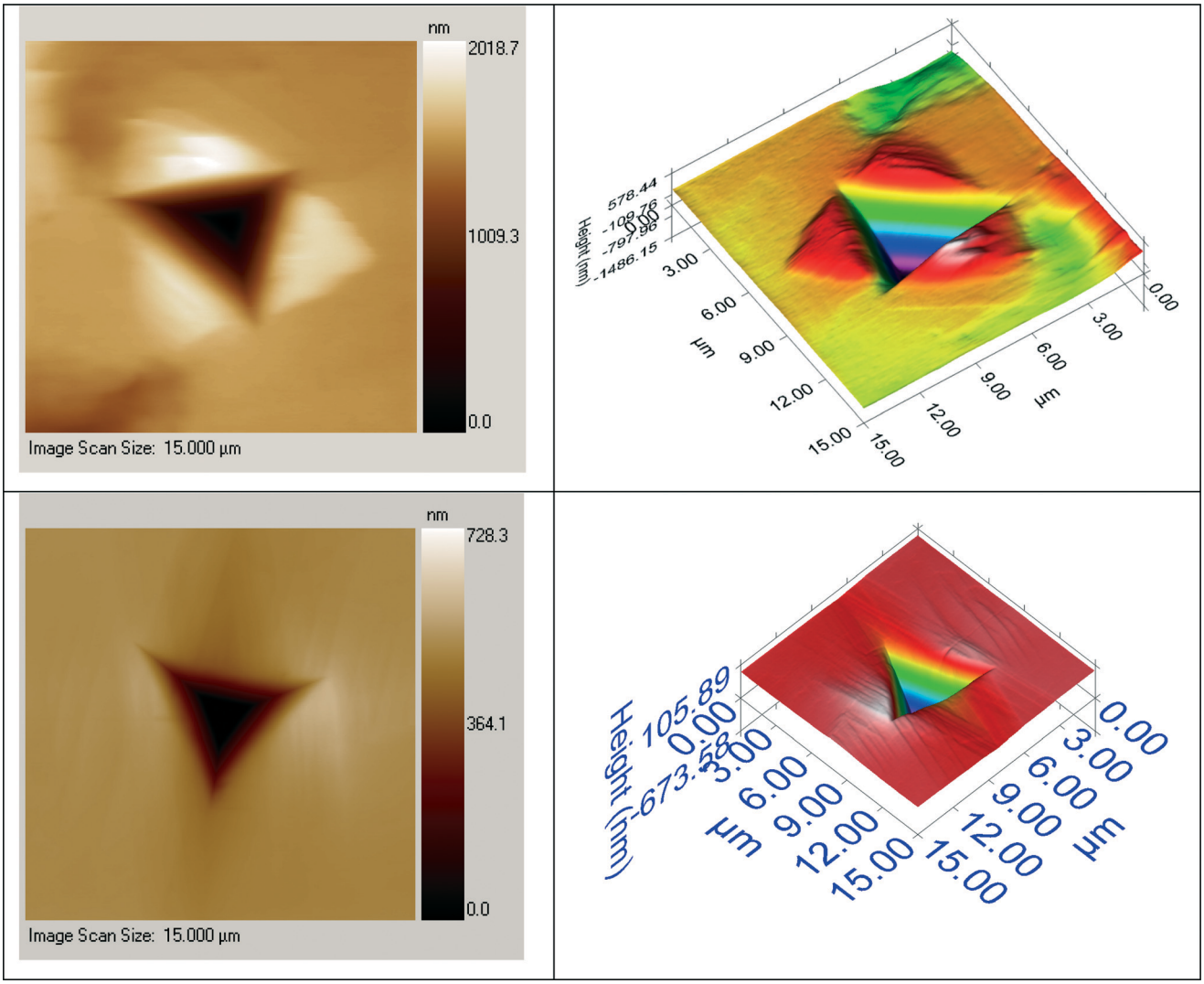

Fig. 2 (Top left) Plan view and (top right) the corresponding 3D AFM image of the (011) face of a sodium saccharin crystal indented with a cube-corner tip, illustrating pile-up due to plastic flow around the indenter. (Bottom left) Plan view and (bottom right) the corresponding 3D AFM image of the residual indent obtained on the (020) face of 1 : 1 complexes of 1,2,4,5-tetracyanobenzene (TCNB) with phenanthrene, showing no pile-up around the indent. (Images courtesy of MSRN Kiran.)

cases, a simple and direct way to estimate H is by dividing P_{max} by the area of the indent, the latter obtained from the scanned images, if available. In the absence of indent images, the methodologies proposed in ref. 27–29 can be explored.

3.2. Fracture toughness

Even before the advent of nanoindentation, indentation testing was widely used to measure the fracture toughness of brittle materials, such as glasses and ceramics.[30] This method is attractive largely because of its simplicity, as the preparation of specimens, whose sizes are large and geometries are often complex, for conventional fracture toughness testing is circumvented. To measure K_i, materials are indented with a sharp pyramidal tip such that cracks emanate from the corners of the indent. (It is important to note here that if the solid does not crack, which would be the case in ductile materials, estimation of K_i is not possible. Hence, K_i can only be estimated for brittle and semi-brittle solids using nanoindentation.) In the early 1980s, Lawn and colleagues[31,32] suggested a relation for estimating K_i through Vickers indentation, based on the half-penny crack configuration:

$$K_i = \alpha \left(\frac{E}{H}\right)^{\frac{1}{2}} \frac{P}{c^{3/2}} \quad (5)$$

where c is the radial crack length from the indentation center to the crack tip, and α is a constant for a given indenter. Although a multitude of other formulae have been proposed,[30,33] eqn (5) remains the most popular. Pronton and Rawlings[34] examined 19 different Vickers indentation toughness equations, and found that most of them have an accuracy of the order of 30% with minor variations.

With the development of nanoindentation, it was revealed that eqn (5) could also be applied to the commonly used three-sided Berkovich indenter, even though there is an important difference – in terms of symmetry – between the Vickers and Berkovich indenters.[35] A particular advantage of nanoindentation is that E and H can be measured with the same set-up. (It is important to note that the estimation of E has to be carried out with a separate test where P_{max} is kept below that required for cracking.) However, due to the fact that very small loads are applied in nanoindentation, cracking may not occur even in the most brittle materials. To overcome this difficulty, the use of a sharper indenter is recommended whose centerline-to-face angle ψ (such as the one illustrated in Fig. 3) is smaller than 65.3°, typical of the Berkovich indenter. For example, the cube-corner indenter, with ψ = 35.3°, was found to be extremely effective for radial crack initiation at very small loads and is now popular for use in toughness estimation in small volumes and thin films.[36] Fig. 4 shows the indentation made in soda-lime glass with an indenter that had ψ = 55°. When three-sided pyramidal indenters with other angles are employed in the cracking studies, the theoretical value of the proportionality coefficient α in eqn (5) can be estimated using the following relation:[36]

$$\alpha_{th} = \frac{0.0352}{(1-\nu)}(\cot\psi)^{\frac{2}{3}}. \quad (6)$$

While K_i measurement using nanoindentation is quite effective, it is pertinent to note that some important questions, two of which are listed below, remain unanswered. (a) How can a half-penny-shaped crack system be operative for three-sided pyramidal indentation despite the difference in symmetry? (b) Is there a more precise expression for the stress intensity factor for three-sided pyramidal indentation?

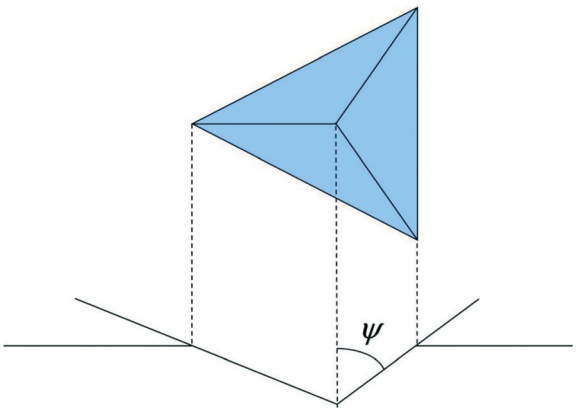

Fig. 3 Schematic illustration of the centerline-to-face angle for a three-sided pyramidal indenter.

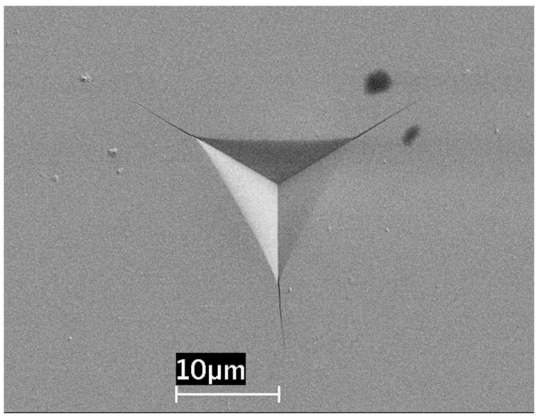

Fig. 4 An indentation in soda-lime glass showing well defined radial cracks.

3.3. Stress–strain responses

While H is a good indicator of a material's resistance to plastic deformation, it is only qualitative, and hence cannot be utilized for engineering design. For such design, parameters including the yield strength, σ_y, and work hardening exponent, n, would be essential. Estimation of these parameters is an easy task for data measured through uniaxial tensile or compression tests, where the stress state is uniform throughout the specimen gage-section. However, deciphering the indentation data is complicated due to the inhomogeneous nature of the stress distribution underneath the indenter.[37,38] Consequently, several attempts have been made, many of which are based on the well-known relationship between hardness, H, and flow stress, σ_f, which is the stress at a characteristic or representative value of the plastic strain, ε_R, originally suggested by Tabor:[39,40]

$$H = C_\theta \cdot \sigma_f \quad (7)$$

where C_θ is the 'constraint factor' which not only depends on the half-angle of a conical indenter, θ, but also on the level of plasticity attained underneath the indenter. In the 'fully plastic' regime, C_θ ranges between 2.6 and 3.0, but in cases where plasticity is pressure sensitive, it can be higher than 3.[41–43] Under certain circumstances, there can be a significant influence from the (E/σ_y) ratio on C_θ. Johnson[44] showed that when deformation is not fully plastic, *i.e.*, in the elastic–plastic transition range, C_θ increases as E/σ_y increases (Fig. 5), and decreases as the indenter angle increases according to the relation:

$$C_\theta = \frac{2}{3}\left[1 + \ln\left(\frac{E}{\sigma_y}\cdot\cot\theta\right)\right] \quad (8)$$

Additionally, he estimated – by employing the expanding cavity analogy for the stress-fields underneath the indenter – ε_R for conical indenters as

$$\varepsilon_R = 0.2\cdot\cot\theta. \quad (9)$$

To apply eqn (9) to the triangular pyramidal indentation data, it is useful to make the normal assumption that similar

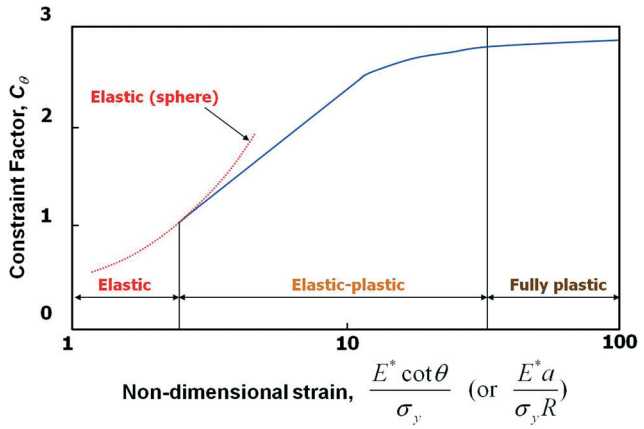

Fig. 5 Constraint factor *vs.* non-dimensional strain during spherical indentation.

behavior is obtained when the angle of the conical indenter gives the same area-to-depth ratio as the three-sided-pyramid indenter, which gives the relation between θ and the centerline-to-face angle ψ as $\theta = \tan^{-1}\left(\sqrt{\frac{3\sqrt{3}}{\pi}}\tan\psi\right)$; *e.g.*, a ψ of 65.3° in Berkovich or Vickers indenters corresponds to a θ of 70.3°. Therefore, $\varepsilon_R \approx 0.072$ for a Berkovich or Vickers indenter (Tabor suggested it to be 0.08).[39] In the case where a spherical tipped indenter is used, $\cot\theta$ in eqn (9) can be replaced by a/R (where a is the contact radius and R is the radius of the tip).[44]

Thus, with the values estimated from eqns (7) and (9), one may be able to extract the uniaxial elastic–plastic constitutive behavior of a solid from the instrumented indentation data. While attempts at this were made from the data obtained by using only one sharp indenter,[45] it was shown that there are associated uniqueness issues, as materials with different combinations of elastic–plastic properties can yield identical *P*–*h* curves.[46] Consequently, the use of dual (or plural) sharp indenters has been suggested to circumvent this problem.[47–50] However, this is still an unresolved issue in the contact mechanics literature.[51]

While obtaining the full stress–strain response may not be straightforward, it is possible to obtain the critical shear stress for the onset plasticity, *i.e.*, yielding, by employing a spherical or any other blunt indenter followed by careful analysis of the measured *P*–*h* curves.[52–54] Fig. 6(a) shows an example of a *P*–*h* curve recorded during spherical indentation of a single crystal at a relatively low peak load. The loading part of the curve is completely reversed upon unloading, indicating that the deformation is perfectly elastic. This elastic *P*–*h* behavior can be described by Hertzian contact theory using:[44,52]

$$P = \frac{4}{3} E_r \sqrt{R} \cdot h^{\frac{3}{2}} \qquad (10)$$

The value of R can be verified using eqn (10) by performing indentations on a sample with a known E_r (such as fused silica or tungsten). Note that the manufacturer-quoted R value can change due to wear of the tip upon repeated usage.

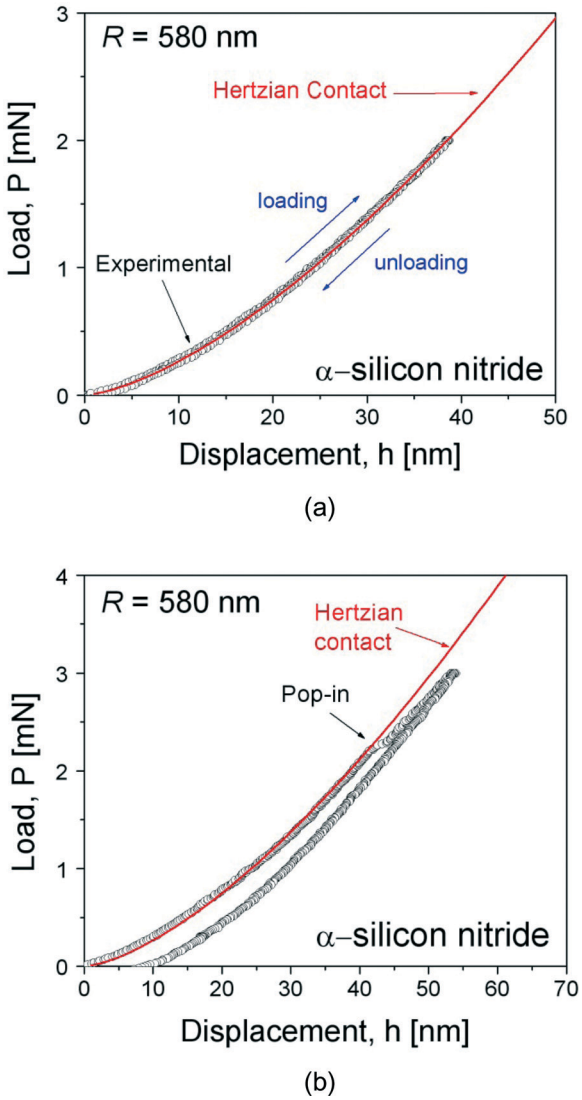

Fig. 6 Nanoindentation load–displacement curves showing: (a) perfectly elastic behavior below the first pop-in load; and (b) pop-in during loading and permanent deformation after unloading.

Fig. 6(b) shows a *P*–*h* curve recorded at a somewhat higher load than the load for Fig. 6(a). A sudden displacement excursion or 'pop-in' is observed during the loading sequence, and upon unloading, the displacement was not fully recovered, thus suggesting that the pop-in corresponds to the elastic–plastic transition, *i.e.*, yielding and the onset of plasticity. It has been reported that the higher the pop-in load, the larger the pop-in displacement,[53,55] which suggests that, at the pop-in event, the indenter displacement jumps from purely elastic Hertzian contact to a *P*–*h* curve more representative of elastic–plastic contact, and that, for a given R, the physical nature of the elastic–plastic transition does not vary with the load level or loading rate.

Since the first pop-in event is caused by the elastic–plastic transition, the maximum shear stress, τ_{max}, at pop-in

represents the critical shear yield strength, σ_c. For Hertzian contact, the maximum shear stress occurs at a distance approximately half of the contact radius directly below contact on the axis of symmetry. The magnitude of this shear stress is given by[44,52]

$$\tau_{max} = 0.31p_0 = 0.31\left(\frac{3}{2}p_m\right) = 0.31\left(\frac{6E_r^2}{\pi^3 R^2}P\right)^{\frac{1}{3}} \quad (11)$$

where p_0 and p_m are the maximum and mean pressures of the contact, respectively. The estimated values in the literature are often of the same order as the theoretical shear strength of a defect-free material, which is typically estimated as $G/2\pi$ or $G/10$.[5,56] In such cases, it has been suggested that the first pop-ins are indeed associated with the homogeneous nucleation of dislocations rather than the activation of pre-existing ones. It is noteworthy that the shear yield stress values generally exhibit wide fluctuations due to the natural inhomogeneities in a material. Thus, statistical analyses of the data may indeed throw more light on underlying deformation mechanisms.[57,58]

In organic and MOF crystals, the magnitudes of pop-ins, $\Delta h_{pop\text{-}in}$, often follow a systematic pattern (see Fig. 7 for a representative P–h curve with several pop-ins). Hence, $\Delta h_{pop\text{-}in}$ often tends to be an integer multiple of some underlying structural parameter and a geometric parameter, which relates the indentation direction with the plane and direction of the crystallographic shear. Such correlations along with knowledge of the close packed planes and directions allow for inferences to be made towards which slip system is operative during plastic deformation of the crystals. In some cases – such as in aspirin – one may also be able to understand the stability of various polymorphic forms under the applied loads.[16] If the material is susceptible to pressure-induced phase transformations, one could observe a phenomenon known as 'pop-out' in the unloading part of the P–h curve as

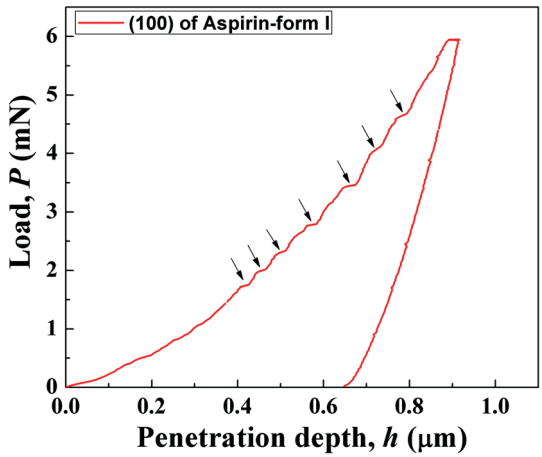

Fig. 7 Representative P–h curve obtained on the (100) face of Form I Aspirin, obtained using a three sided pyramidal indenter, showing several pop-ins, which are indicated by arrows. (Plot courtesy of MSRN Kiran.)

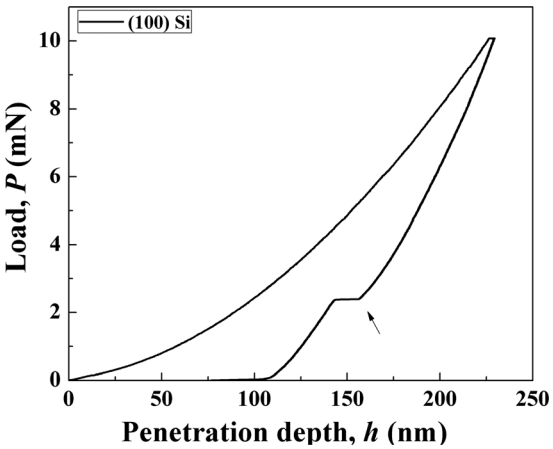

Fig. 8 Representative P–h curve obtained on the (100) face of single crystal Si, obtained using a three sided pyramidal indenter. Pop-out during unloading is identified by the arrow.

shown in Fig. 8.[59] Here, just as in pop-ins, a sudden displacement jump at constant load (in the load-controlled tests) occurs. These pop-outs occur due to sudden changes in the volume of the material – associated with stress induced phase transformations – and careful analysis of the load at which these pop-outs occur could throw light on the pressure at which such transformations occur.

3.4. Time-dependent properties

The time-dependent 'plastic' deformation of a material, often referred to as creep, can also be examined using nanoindentation. The steady-state creep strain rate, $\dot{\varepsilon}_{ss}$, is sensitive to the applied stress, σ, and varies according to the equation: $\dot{\varepsilon}_{ss} = \zeta(\sigma)^n$. Here, ζ is a material and temperature dependent factor, and n $(= \partial \ln \dot{\varepsilon}/\partial \ln \sigma)$ is the creep stress exponent. The value of n often indicates the rate-controlling deformation mechanism.[5] Since the stress and strain states during indentation are not single-valued, the strain rate, $\dot{\varepsilon}$, and σ are estimated in an approximate fashion. While σ is obtained from the hardness with the aid of eqn (9), $\dot{\varepsilon}$ for a sharp indenter is given by:[60]

$$\dot{\varepsilon} = \frac{1}{h}\frac{dh}{dt} = \frac{\dot{h}}{h} \quad (12)$$

The creep behavior of a material can be examined using the nanoindentation technique by keeping any of the following experimental parameters constant during the test: maximum displacement, loading-rate, strain-rate or maximum load.[61–66] Amongst these, the constant load test is the most popular due to its close resemblance to the conventional uniaxial creep test. In this method, the sample is quickly loaded to a predetermined peak load, then the load is held constant and the increase in h with hold time, t, is monitored. From the h *vs.* t data, the change in σ with t can be estimated. To estimate the displacement rate (dh/dt), which is required

for computing $\dot{\varepsilon}$, the h–t data is fitted with an empirical equation:[67]

$$h(t) = h_0 + Et^{\kappa} + \Phi t \quad (13)$$

where h_0 is the indentation depth at $t = 0$, and E, Φ, and κ are fitting constants. Finally, by plotting σ *vs.* $\dot{\varepsilon}$ on a log–log scale, n can be obtained.

However, certain limitations of the nanoindentation technique for evaluating creep, especially when a sharp tip is utilized, should be kept in mind. Firstly, the characteristic indentation strain $\varepsilon_{\text{char}}$ (that is the strain comparable to uniaxial flow strain) is defined by eqn (9), and for a sharp tip, β, and thus the strain is fixed and independent of creep displacement due to the geometrical self-similarity of the indenter, while the creep strain *vs.* time curve is the key data in uniaxial creep tests. Secondly, from the continuum plasticity viewpoint, the characteristic stress underneath a given sharp tip is unique, which makes it virtually impossible to plot the change in strain rate as a function of stress. Therefore, in the constant load method, the change in h during a load-hold sequence is used for calculating the stress variation. In uniaxial creep tests, the σ for calculating n is not the varying stresses in the load-hold sequence but the initial stress at the onset of creep, and thus a large number of tests at different initial stress levels are required for determining the n value. This concept cannot be applied to the constant-load sharp indentation creep method unless multiple tips with different angles are used for the experiments. Thirdly, the unique characteristic stress must be plastic due to the singularity issue of the tip (if the tip is not blunted). This may induce a difference from the uniaxial creep data, for which applied stress is elastic. Fourthly, high stress underneath the indenter can induce a much higher strain rate than that observed during conventional uniaxial creep. This makes it difficult to find a proper creep mechanism. One of the possible ways to overcome some of the above-mentioned problems is to perform the constant-load nanoindentation creep tests using a spherical indenter.[67,68] In spherical indentation, the $\varepsilon_{\text{char}}$ as well as the σ (*i.e.*, H) at the onset of creep can be systematically varied by simply changing the applied peak load, $P_{\max}$ (with a fixed r). Thus, one can study the material's response in elastic, elasto-plastic, and then fully-plastic regimes.

4. Additional options and possibilities

A number of options – in addition to those discussed in section 3 – that make the nanoindentation technique more versatile for probing a material's behavior are now becoming available. These are briefly mentioned below.

Micro-pillar compression experiments

As mentioned already, the stress state underneath an indenter is inhomogeneous and complex, and hence deciphering the test results is not always straightforward. Therefore, uniaxial compression or testing is preferable. This is easy if sufficient material is available. If the material is only available in small volumes, specimens which resemble micro-pillars can be synthesized, either through techniques such as focused ion beam (FIB) milling or through direct synthesis. These micron or sub-micron sized pillars can then be compressed with a nanoindenter equipped with a flat punch tip. This technique – known as micropillar compression – has become popular in the recent past, especially for assessing the effects of size on the strength of a wide variety of materials.[69–72]

Mechanical property measurement with the aid of an atomic force microscope (AFM)

It is possible – sometimes – to utilize an AFM equipped with a sharp and stiff tip to probe the mechanical properties of materials (see Chow *et al.*'s recent review[73] on this topic). Since AFM is intrinsically built to measure force as a function of displacement, this appears to be a natural consequence. One of the great advantages of the AFM-indentation technique is that it can be utilized on much smaller and softer samples for which nanoindentation would be 'too coarse' a technique. However, this technique suffers from the fact that AFMs are typically built such that the load-train is extremely compliant, which allows for large displacements of the tip with varying electro-static attractive and repulsive forces experienced by the tip and the material being probed. Thus, in the indentation mode, the measured displacement is more than likely to contain a substantial amount of displacement associated with deformation/deflection of the instrument. This makes accurate estimation of mechanical properties difficult.

Nanoindentation at high/low temperatures

Most of the nanoindentation experiments reported in literature – to date – were performed at room temperature. Naturally, it would be advantageous to measure properties as a function of temperature, which in turn would give insights into aspects like phase stability and structural phase transformations with temperature. While nanoindenters equipped with high temperature stages are now available, the maximum temperatures that one can attain are not very high (of the order of a few hundred °C). This is as a result of the need to keep the thermal drift to an absolute minimum, which becomes a huge task at higher temperatures. Ensuring that the tip and the specimen are at the same temperature is a challenge as well. The tips are likely to wear much more quickly at high temperatures. At sub-ambient temperatures, water condensation on the sample could influence the measured P–h responses, and hence the specimen and indenter chamber has to be kept absolutely dry.

Simultaneous measurement of the electrical contact resistance (ECR)

In many materials, structural phase transformations, plasticity events, dislocation emissions, and fracture events such as

cracking and/or delamination from the substrate are associated with changes in the intrinsic electrical flow resistance. Thus, if a electrically conducting tip is used, it is possible – with a suitable electrical circuit – to keep track of the changes to the ECR of the material during nanoindentation. This would enable one to estimate the stress at which these events take place.[74–78]

Monitoring of acoustic emission during indentation

Just as in the ECR technique, it is possible to monitor the acoustic signals that emanate during nanoindentation (see Faisal *et al.*'s recent review[79] on this topic for further details). Since many of the phase transformations, deformations and fracture events are typically associated with sudden spurts of energy release, which in turn get dissipated as acoustic waves, monitoring of the acoustic signals can provide additional and detailed information about what happens under the indenter during nanoindentation.

Nanoscratch studies

Typically, indentation – at all scales – is performed in such a way that the indenter's penetration into the sample is normal to the surface being indented. However, with some nanoindenters it is possible to glide or 'scratch' the surface. This can be done in two ways: one is to scratch with a constant applied load, the other is glide while the load is increased as a function of the sliding distance. Nanoscratch tests are ideally suited for testing the adhesion of coatings to substrates or friction coefficients of surfaces. In the context of organics, the test can be utilized for understanding molecular migration in layered crystals as demonstrated in ref. 15.

In-situ indentation to understand real-time contact induced deformation

Most nanoindentation measurements are performed *ex-situ*, *i.e.*, the *P–h* curves are collected and the images of the indents are collected *post-facto* (images too are only collected in some selected cases). Naturally, one has to construe – on . the basis of the *P–h* responses and the indenter impressions – what happened during indentation. Thus, nanoindentation inside either a scanning or transmission electron microscope could be more informative. While such *in-situ* indentation allows imaging of surface features when performed inside a scanning electron microscope, one could visualize plastic deformation mechanisms using a transmission electron microscope.[80]

5. Summary and outlook

Nanoindentation is fast emerging as the technique of choice for probing the mechanical behavior of a wide variety of materials. Because of its capability for testing very small volumes of materials, it is particularly useful for unraveling the structure–mechanical property correlations that would aid crystal engineering in terms of furthering our understanding of molecular interactions and their influence on crystal packing. Early work has already demonstrated that nanoindentation is useful for gaining new insights into a variety of aspects associated with organic and inorganic crystals. Since nanoindentation also measures physical properties in nature, it can be utilized gainfully to correlate with other physical properties and in the process learn a great deal more about the crystal under investigation. Once such connections are established, nanoindentation may – in some instances – turn out to be a useful and quick quality control method, and here lies the most promising aspect of this technique. In this paper, we have made an attempt – in as brief and yet lucid manner as possible – to describe the technique and the various experimental parameters that can be employed, how the data can be analyzed in order to estimate various mechanical properties, and the advantages and the pitfalls that one should avoid. We believe that this technique would allow for structural–mechanical property correlations to be firmly established within the context of crystal engineering, which in turn would enable chemists to understand and design certain functional properties which are influenced by stress.

Acknowledgements

The work at IISc was sponsored by the Department of Science and Technology, Government of India. The work at Hanyang University was supported by the Human Resources Development program (No. 20114010203020) of the Korea Institute of Energy Technology Evaluation and Planning (KETEP) grant funded by the Korea government Ministry of Trade, Industry and Energy. UR thanks GR Desiraju, MSRN Kiran, S. Varughese, MK Mishra, CM Reddy, and W. Li for collaboration and discussions on nanoindentation of organic crystals and MOFs.

References

1 J. Boussinesq, *Applications des Potentiels a l'etude de equilibre et du mouvement des solides elastiques*, Gauthier-Villars, Paris, 1885.
2 H. Hertz, *J. Reine Angew. Math.*, 1882, **92**, 156–171.
3 A. Wahlberg, *J. Iron Steel Inst.*, 1901, **59**, 243–298.
4 E. Meyer, *Z. ver. Deut. Ing.*, 1908, **52**, 645–654.
5 G. E. Dieter, *Mechanical Metallurgy*, McGraw-Hill Book Company, London, 1988.
6 S. I. Bulychev, V. P. Alekhin, M. Kh. Shorshorov, A. P. Ternovskii and G. D. Shnyrev, *Zavod. Lab.*, 1975, **41**, 1137–1140.
7 J. B. Pethica, R. Hutchings and W. C. Oliver, *Philos. Mag. A*, 1983, **48**, 593–606.
8 J. L. Loubet, J. M. Georges, O. Marchesini and G. Meille, *Trans. ASME, J. Tribol.*, 1984, **106**, 43–48.
9 ISO 14577, Part 1–4, Metallic materials – Instrumented indentation test for hardness and materials parameters, 2002, (for Part 1–3), 2007, (for Part 4), ISO.
10 ASTM E2546-07, *Standard Practice for Instrumented Indentation Testing*, 2007, ASTM International.

11 (*a*) J. C. Tan, J. D. Furman and A. K. Cheetham, *J. Am. Chem. Soc.*, 2009, **131**, 14252–14254; (*b*) J. C. Tan and A. K. Cheetham, *Chem. Soc. Rev.*, 2011, **40**, 1059–1080; (*c*) G. Rama Krishna, M. S. R. N. Kiran, C. L. Fraser, U. Ramamurty and C. Malla Reddy, *Adv. Funct. Mater.*, 2013, **23**, 1422–1430; (*d*) W. Li, M. S. R. N. Kiran, J. L. Manson, J. A. Schlueter, A. Thirumurugan, U. Ramamurty and A. K. Cheetham, *Chem. Commun.*, 2013, **49**, 4471–4473; (*e*) M. K. Mishra, S. Varughese, U. Ramamurty and G. R. Desiraju, *J. Am. Chem. Soc.*, 2013, **135**, 8121–8124; (*f*) W. Li, P. T. Barton, M. S. R. N. Kiran, R. P. Burwood, U. Ramamurty and A. K. Cheetham, *Chem.–Eur. J.*, 2011, **17**, 12429–12436.

12 (*a*) T. D. Bennett, D. A. Keen, J.-C. Tan, E. R. Barney, A. L. Goodwin and A. K. Cheetham, *Angew. Chem., Int. Ed.*, 2011, **123**, 3123–3127; (*b*) C. M. Reddy, R. C. Gundakaram, S. Basavoju, M. T. Kirchner, K. A. Padmanabhan and G. R. Desiraju, *Chem. Commun.*, 2005, 3945–3947; (*c*) M. S. R. N. Kiran, S. Varughese, C. M. Reddy, U. Ramamurty and G. R. Desiraju, *Cryst. Growth Des.*, 2010, **10**, 4650–4655; (*d*) S. Sahoo, S. Sinha, M. S. R. N. Kiran, U. Ramamurty, A. Dericioglu, C. M. Reddy and P. Naumov, *J. Am. Chem. Soc.*, 2013, **135**, 13843–13850; (*e*) J. C. Tan, C. A. Merrill, J. B. Orton and A. K. Cheetham, *Acta Mater.*, 2009, **57**, 3481–96.

13 C. Karunatilaka, D.-K. Bucar, L. R. Ditzler, T. Friscic, D. C. Swenson, L. R. MacGillivray and A. V. Tivanski, *Angew. Chem., Int. Ed.*, 2011, **50**, 8642–8646.

14 S. Varughese, M. S. R. N. Kiran, U. Ramamurty and G. R. Desiraju, *Angew. Chem., Int. Ed.*, 2013, **52**, 2701–2712.

15 S. Varughese, M. S. R. N. Kiran, U. Ramamurty and G. R. Desiraju, *Chem.–Asian J.*, 2012, **7**, 2118–2125.

16 S. Varugese, M. S. R. N. Kiran, A. D. Bond, K. Solonko, U. Ramamurty and G. R. Desiraju, *Chem. Sci.*, 2011, **2**, 2236–2242.

17 F. Gallego-Gomez, V. Morales-Florez, A. Blanco, N. de la Rosa-Foz and C. Lopez, *Nano Lett.*, 2012, **12**, 4920–4924.

18 K. Altaf, I. A. Ashcroft and R. Hague, *J. Mater. Sci.*, 2011, **46**, 7551–7557.

19 M. S. R. N. Kiran, S. Varugese, U. Ramamurty and G. R. Desiraju, *CrystEngComm*, 2012, **14**, 2489–2493.

20 G. M. Pharr, E. G. Herbert and Y. Gao, *Annu. Rev. Mater. Res.*, 2010, **40**, 271–292.

21 W. D. Nix and H. Gao, *J. Mech. Phys. Solids*, 1998, **46**, 411–425.

22 I.-C. Choi, Y. Zhao, Y.-J. Kim, B.-G. Yoo, J.-Y. Suh, U. Ramamurty and J.-I. Jang, *Acta Mater.*, 2012, **60**, 6862–6868.

23 W. C. Oliver and G. M. Pharr, *J. Mater. Res.*, 1992, **7**, 1564–1583.

24 I. N. Sneddon, *Int. J. Eng. Sci.*, 1965, **3**, 47–57.

25 G. Simmons and H. Wang, *Single Crystal Elastic Constants and Calculated Aggregate Properties: A Handbook*, 2nd edn, The M.I.T. Press, Cambridge, MA, 1971 .

26 G. M. Pharr, W. C. Oliver and F. R. Brotzen, *J. Mater. Res.*, 1992, **7**, 613–617.

27 Y.-T. Cheng and C.-M. Cheng, *Appl. Phys. Lett.*, 1998, **73**, 614–616.

28 D. L. Joslin and W. C. Oliver, *J. Mater. Res.*, 1990, **5**, 123–126.

29 W. C. Oliver and G. M. Pharr, *J. Mater. Res.*, 2004, **19**, 3–20.

30 R. F. Cook and G. M. Pharr, *J. Am. Ceram. Soc.*, 1990, **73**, 787–817.

31 B. R. Lawn, A. G. Evans and D. B. Marshall, *J. Am. Ceram. Soc.*, 1980, **63**, 574–581.

32 G. R. Anstis, P. Chantikul, B. R. Lawn and D. B. Marshall, *J. Am. Ceram. Soc.*, 1981, **64**, 533–538.

33 M. Sakai and R. C. Bradt, *Int. Mater. Rev.*, 1993, **38**, 53–78.

34 (*a*) C. B. Pronton and R. D. Rawlings, *Mater. Sci. Technol.*, 1989, **5**, 865–872; (*b*) C. B. Pronton and R. D. Rawlings, *Mater. Sci. Technol.*, 1989, **5**, 961–976.

35 G. M. Pharr, *Mater. Sci. Eng., A*, 1998, **253**, 151–159.

36 J.-I. Jang and G. M. Pharr, *Acta Mater.*, 2008, **56**, 4458–4469.

37 G. Srikant, N. Chollacoop and U. Ramamurty, *Acta Mater.*, 2006, **54**, 5171–78.

38 K. Eswar Prasad, N. Chollocoop and U. Ramamurty, *Acta Mater.*, 2011, **59**, 4343–4355.

39 D. Tabor, *The hardness of metals*, Oxford University Press, Oxford, 1951 .

40 A.G. Atkins and D. Tabor, *J. Mech. Phys. Solids*, 1970, **13**, 149.

41 M. N. M. Patnaik, R. Narasimhan and U. Ramamurty, *Acta Mater.*, 2004, **52**, 3335–3345.

42 V. Keryvin, K. Eswar Prasad, Y. Gueguen, J.-C. Sangleboeuf and U. Ramamurty, *Philos. Mag.*, 2008, **88**, 1773–1790.

43 K. Eswar Prasad, V. Keryvin and U. Ramamurty, *J. Mater. Res.*, 2009, **24**, 890–897.

44 K. L. Johnson, *Contact Mechanics*, University Press, Cambridge, Cambridge, 1985.

45 M. Dao, N. Chollacoop, K. J. Van Vliet, T. A. Venkatesh and S. Suresh, *Acta Mater.*, 2001, **49**, 3899–3918.

46 Y.-T. Cheng and C.-M. Cheng, *J. Mater. Res.*, 1999, **14**, 3493–3496.

47 J. L. Bucaille, S. Stauss, E. Felder and J. Michler, *Acta Mater.*, 2003, **51**, 1663–1678.

48 N. Chollacoop, M. Dao and S. Suresh, *Acta Mater.*, 2003, **51**, 3713–3729.

49 S. Shim, J.-I. Jang and G. M. Pharr, *Acta Mater.*, 2008, **56**, 3824–3832.

50 N. Chollacoop and U. Ramamurty, *Scr. Mater.*, 2005, **53**, 247–251.

51 X. Chen, N. Ogasawara, M. Zhao and N. Chiba, *J. Mech. Phys. Solids*, 2007, **55**, 1618–1660.

52 T. F. Page, W. C. Oliver and C. J. McHargue, *J. Mater. Res.*, 1992, **7**, 450–473.

53 C. A. Schuh, J. K. Mason and A. C. Lund, *Nat. Mater.*, 2005, **4**, 617–621.

54 H. Bei, Z. P. Lu and E. P. George, *Phys. Rev. Lett.*, 2004, **93**, 125504.

55 J.-I. Jang, H. Bei, P. F. Becher and G. M. Pharr, *J. Am. Ceram. Soc.*, 2012, **95**, 2113–2115.

56 J. Frenkel, *Z. Phys.*, 1926, **37**, 572–609.

57 C. E. Packard, O. Franke, E. R. Homer and C. A. Schuh, *J. Mater. Res.*, 2010, **25**, 2251–2263.

58 I.-C. Choi, Y. Zhao, Y.-J. Kim, B.-G. Yoo, J.-Y. Suh, U. Ramamurty and J.-I. Jang, *Acta Mater.*, 2012, **60**, 6862–6868.
59 J.-I. Jang, M. J. Lance, S. Wen, T. Y. Tsui and G. M. Pharr, *Acta Mater.*, 2005, **53**, 1759–1770.
60 B. N. Lucas and W. C. Oliver, *Metall. Mater. Trans. A*, 1999, **30**, 601–610.
61 W. R. LaFontaine, B. Yost, R. D. Black and C.-Y. Li, *J. Mater. Res.*, 1990, **5**, 2100.
62 M. J. Mayo and W. D. Nix, *Acta Metall.*, 1988, **36**, 2183.
63 M. J. Mayo, R. W. Siegel, A. Narayanasamy and W. D. Nix, *J. Mater. Res.*, 1990, **5**, 1073.
64 R. Goodall and T. W. Clyne, *Acta Mater.*, 2006, **54**, 5489–5499.
65 D. S. Stone, J. E. Jakes, J. Puthoff and A. A. Elmustafa, *J. Mater. Res.*, 2010, **25**, 611–621.
66 I.-C. Choi, B.-G. Yoo, Y.-J. Kim and J.-I. Jang, *J. Mater. Res.*, 2012, **27**, 3–11.
67 I.-C. Choi, B.-G. Yoo, Y.-J. Kim, M.-Y. Seok, Y. Wang and J.-I. Jang, *Scr. Mater.*, 2011, **65**, 300–303.
68 B.-G. Yoo, K.-S. Kim, J.-H. Oh, U. Ramamurty and J.-I. Jang, *Scr. Mater.*, 2010, **63**, 1205–1208.
69 J. R. Greer and J. Th. M. De Hosson, *Prog. Mater. Sci.*, 2011, **56**, 654–724.
70 A. Dubach, R. Raghavan, J. F. Löffler, J. Michler and U. Ramamurty, *Scr. Mater.*, 2009, **60**, 567–570.
71 A. Dubach, K. Eswar Prasad, R. Raghavan, J. F. Löffler, J. Michler and U. Ramamurty, *J. Mater. Res.*, 2009, **24**, 2697–704.
72 R. Raghavan, K. Boopathy, R. Ghisleni, M. A. Pouchon, U. Ramamurty and J. Michler, *Scr. Mater.*, 2010, **62**, 462–465.
73 E. H. H. Chow, D.-K. Bučar and W. Jones, *Chem. Commun.*, 2012, **48**, 9210–9226.
74 V. V. Shastry and U. Ramamurty, *Acta Mater.*, 2013, **61**, 5119–5129.
75 M. S. R. N. Kiran, U. Ramamurty and A. Mishra, *Nanotechnology*, 2013, **24**, 015707.
76 H. H. Nguyen, P. J. Wei and J. F. Lin, *Adv. Nat. Sci.: Nanosci. Nanotechnol.*, 2011, **2**, 015007.
77 J. E. Bradby, J. S. Williams and M. V. Swain, *Phys. Rev. B: Condens. Matter*, 2003, **67**, 085205.
78 S. Sridhar, A. E. Giannakopoulos, S. Suresh and U. Ramamurty, *J. Appl. Phys.*, 1999, **85**, 380–387.
79 N. H. Faisal, R. Ahmed and R. L. Reuben, *Int. Mater. Rev.*, 2011, **56**, 98–142.
80 A. M. Minor, S. A. Syed Asif, Z. Shan, E. A. Stach, E. Cyrankowski, T. J. Wyrobek and O. L. Warren, *Nat. Mater.*, 2006, **5**, 697–702.